PAPER

Uniform carbon-coated CdS core–shell nanostructures: synthesis, ultrafast charge carrier dynamics, and photoelectrochemical water splitting†

Sancan Han,[a] Ying-Chih Pu,[b] Lingxia Zheng,[a] Linfeng Hu,[a] Jin Zhong Zhang*[b] and Xiaosheng Fang*[a]

Photoelectrochemical (PEC) water splitting using solar energy has received widespread attention, and strong performance photocatalysts are highly desired. In this work, uniform carbon-coated CdS nanostructures have been fabricated using ascorbic acid as the carbon source by a facile hydrothermal method and characterized using transmission electron microscopy (TEM). The thickness of the carbon layer can be well controlled by the amount of ascorbic acid added during the reaction. Compared to pristine CdS, carbon-coated CdS nanostructures exhibit stronger light absorption and more efficient electron transfer as determined by absorption and photoluminescence (PL) spectroscopy. Ultrafast charge carrier dynamics in the composite CdS/C structures were studied using femtosecond transient absorption (TA) spectroscopy, which revealed direct evidence of effective charge transfer from CdS to the carbon layer. In addition, the CdS/C composites were employed as photoanodes for PEC hydrogen generation, which showed significant improvement in photoactivity over pristine CdS nanospheres. The photocurrent density (−1.0 V *vs.* Ag/AgCl) of one of the composite structures, CdS/7-C, exhibited ∼20 times enhancement compared with that of pristine CdS. The enhanced PEC property can be attributed to increased light scattering and consequently the light harvesting throughout the whole spectral wavelength, and the effective electron transfer from CdS to the carbon layer. Such carbon-coated semiconductor composites based on a simple and low-cost synthesis method should be useful in PEC as well as other applications such as photovoltaics, detectors and sensors.

1. Introduction

Water splitting utilizing solar energy has been a topic of strong interest in the field of renewable energy. In particular, photoelectrochemical (PEC) water splitting using nanoscaled semiconductor photocatalysts has received significant attention.[1–6] Among them, cadmium sulfide (CdS) with a direct bandgap of ∼2.4 eV has absorption matching well with the spectrum of sunlight and also owing to its other useful properties such as excellent charge carrier transport, relatively low work function, good chemical and thermal stability is considered as an excellent material for PEC applications.[7–12] Despite these advantages, one limitation is its generally low PEC conversion efficiencies due to fast charge carrier recombination. Therefore, much effort has been made to effectively reduce recombination of

charge carriers.[13–16] For example, Wu *et al.* have demonstrated that a CdS–Pt heterostructure can provide a possible way for optimizing the hole transfer step to achieve efficient solar-to-fuel conversion.[17] Li *et al.* reported that the combination of enhanced charge transfer and broad light absorption was responsible for improved hydrogen generation in the sandwich-structured CdS–Au–TiO$_2$ nanorod arrays as photoanodes in PEC.[18] However, these semiconductor-layers and plasmonic-metal layers (mainly silver and gold) tend to self-agglomerate, which increases the recombination of electrons and holes.

Carbon materials exhibit excellent electrical conductivity,[19] superior chemical and electrochemical stability,[20] unique physical properties,[21] and good light response.[22] Intense studies have been focused on graphene/semiconductor composites in photocatalytic and PEC applications.[13,23–29] However, complete and uniform graphene coverage on the semiconductor, which ensures electron transfer in all directions, has been challenging for practical application. Meanwhile, carbon-coated semiconductors with complete and ultrathin carbon layers have been extensively investigated in lithium-ion batteries and photocatalysis,[30–33] Lou *et al.* have firstly evidenced that a carbon-

[a] *Department of Materials Science, Fudan University, Shanghai 200433, P. R. China. E-mail: xshfang@fudan.edu.cn*

[b] *Department of Chemistry and Biochemistry, University of California, Santa Cruz, California 95064, USA. E-mail: zhang@ucsc.edu*

coated CdS nanohybrid exhibits significantly enhanced photo-stability and photocatalytic ability,[33] indicating that thin carbon layers with a degree of graphitization can facilitate electron transfer and prevent the active core materials from contacting with oxygen and moisture in the air. This suggests that carbon layers should be an ideal and promising shell material for coating active semiconductor photocatalysts in PEC applications. However, the report about carbon-coated semiconductors applied for a photoelectrochemical field is scarce. Moreover, to date there are mainly two methods for depositing carbon layers:[34,35] (1) *in situ* pyrolysis of the organic precursor (*e.g.* glucose and citric acid); (2) a chemical vapor deposition (CVD) assisted solid-state route. However, these two approaches usually lead to partial carbon coating or require high temperature annealing (>600 °C) under an inert atmosphere. Therefore, a simple, efficient and low-cost method for the deposition of uniform carbon-coated semiconductors at mild operation temperature is highly desired.

In this work, CdS/C composites were synthesized in high yields using ascorbic acid as the carbon source by a facile two-step hydrothermal method, which produces a uniform, thin carbon layer coating on the CdS surface. The thickness of the carbon layer can be easily controlled by the amount of ascorbic acid in the reaction. The effective electron transfer and more light absorption in CdS/C composites are confirmed by PL, and UV-vis spectroscopy, which could lead to the enhanced photo-activity. According to the PEC study, the carbon-coated CdS electrode indeed shows excellent photoactivity compared with that of pristine CdS. Importantly, the role of the carbon layer on charge carrier dynamics in detail has been investigated using femtosecond transient absorption (TA) spectroscopy, which provides a direct measure of charge carrier dynamics including electron transfer from CdS to the carbon layer. These results show that a uniform and thin layer of carbon material can substantially enhance electron transfer, which leads to the significant enhancement in the photocurrent density compared with that of pristine CdS. Hence, the CdS/C core–shell composites obtained provide promising candidates for high performance PEC and other potential applications, and the facile and low-cost synthetic method can be extended to fabricate other carbon-coated semiconductors.

2. Experimental section

2.1 Materials

All chemicals were used as received without any further purification. $Cd(CH_3COO)_2 \cdot 2H_2O$ (Sinopharm Chemical Reagent Corp.), thiourea (Sinopharm Chemical Reagent Corp.), analytic alcohol (98%, Sigma-Aldrich), and ascorbic acid (Sinopharm Chemical Reagent Corp.).

2.2 Synthesis of CdS/C composites

The synthesis of pristine CdS nanospheres. The CdS nanospheres were fabricated by a modified method described in detail elsewhere.[12] Typically, 2.4 mmol of $Cd(CH_3COO)_2 \cdot 2H_2O$ and 24 mmol of thiourea in 60 mL deionized water, were added

to a 100 mL Teflon-lined stainless steel autoclave, then the autoclave was maintained at 200 °C for 5 h and allowed to cool to room temperature naturally afterwards. Yellow precipitates were collected and washed with deionized water and ethanol three times, respectively. The final products were dried in a vacuum oven at 65 °C for 10 h.

The synthesis of CdS/C composites. Pristine CdS nano-spheres in 30 mL de-ionized water and 30 mL ethanol were stirred for 1 hour. Ascorbic acid was added into the solution to stir for another 1 h, and then it was transferred to a 100 mL Teflon-lined stainless steel autoclave to maintain the temperature at 200 °C for 2 h and cooled down naturally to room temperature. Then the samples were collected by centrifugation and washed with deionized water and ethanol for several times, respectively. The final products were dried in a vacuum oven for 8 h at 60 °C. The pure carbon materials were fabricated without CdS for comparison under the same reaction conditions.

2.3 Characterization

The morphology and the carbon layer thickness were determined by high-resolution transmission electron microscopy (HR-TEM, TECNAI G^2 S-TWIN). X-ray diffraction using Cu Kα radiation (XRD, Bruker D8-A25) was adopted to examine the crystalline structure of the samples. The optical and fluorescence properties of the samples at room temperature were investigated using a UV-vis spectrophotometer (Hitachi U-4100) and photoluminescence (PL) spectrofluorometer (Fluoromax-4). The XPS spectra of the samples were recorded with a Perkin Elmer PHI 5000 C ESCA system equipped with a hemispherical electron energy analyzer, and the Mg-Kα (1253.6 eV) anode was operated at 14 kV and 20 mA. The FT-IR and Raman spectra were collected on a Nexus 470 FT-IR spectrometer and Spex 403 Raman spectrometer.

Ultrafast transient absorption (TA) spectroscopy was carried out with a Quantronix laser system consisting of a Palitra-FS optical parametric amplifier pumped by an Integra-C Ti:sapphire amplifier system, as reported in the previous work.[36] Briefly, 795 nm, 820 mW, and 150 fs pulses from Integra-C were split 9 : 1 between an optical parametric amplifier (OPA) and sapphire crystal, respectively. A pump wavelength of 400 nm (~3.1 eV) was used to excite the samples at 90 nJ per pulse, which could guarantee linear effects. And a white light continuum, which was stable from 430 nm to 800 nm with a pulse width of 100 fs, was used to probe the samples.

2.4 Photoelectrochemical test

The photocurrent of pristine CdS and CdS/C composites electrodes was measured using a Solartron 1280 B (Oakridge, TN) electrochemical workstation in a three-electrode electrochemical cell with a Pt wire as the counter electrode and Ag/AgCl as a reference electrode. In a typical experiment, the potential was swept from −1.2 V to 0 V *vs.* Ag/AgCl at a scan rate of 5 mV s^{-1}. IPCE were measured using a xenon lamp (1000 W) coupled with an infrared water filter (Oriel 6127) and aligned monochromator (Oriel Cornerstone 130 1/8m). The samples were spun on the Fluorine-doped Tin Oxide (FTO) glass (7 Ω

sq^{-1}) and then annealed at 350 °C for 2 h under a nitrogen environment, used as the working electrode with a working area of (~1 cm^2). A 0.25 M Na$_2$S and 0.35 Na$_2$SO$_3$ aqueous solution was used as the electrolyte.

3. Results and discussion

Transmission electron microscopy (TEM) images of CdS coated with a carbon layer at different magnifications are shown in Fig. 1. Fig. 1a and b reveal that a uniform carbon layer is successfully deposited on the surface of the CdS nanospheres. From the high-resolution TEM (HRTEM) images in Fig. 1c and d, the thickness of the amorphous carbon layer is found to be ~3 nm and ~7 nm with the amount of ascorbic acid of 0.001 g and 0.01 g, respectively. Hence the carbon-coated CdS nano-structures are labeled as CdS/3-C and CdS/7-C based on the carbon layer thickness. The TEM results convinced that the carbon deposition was *via* a hydrothermal reaction in which the ascorbic acid was transformed *in situ* into carbon on the surface of CdS, resulting in the carbon-coated CdS composites. The strong interaction between the hydroxyl groups of the carbon layer and Cd^{2+} on CdS results in good contact and large inter-faces between the two components,[37–40] which is desirable for electron transfer from CdS to the carbon layer. The thickness of the carbon layer depends on the amount of ascorbic acid added during the synthesis.

Pure carbon materials were obtained by hydrothermal pyrolysis of ascorbic acid without CdS during the same hydro-thermal reaction, and their morphologies, chemical composi-tion and optical properties were studied for comparison. The TEM images of pure carbon structures are shown in Fig. S1,†
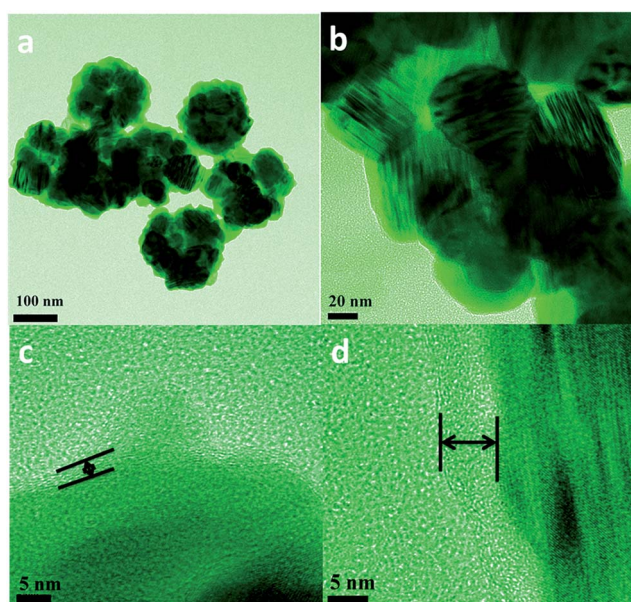

Fig. 1 (a) and (b) Transmission electron microscopy (TEM) images of CdS coated with a carbon layer. (c) High-Resolution TEM (HR-TEM) image of 1 : 100 CdS/C core−shell composites with a carbon layer thickness of ~3 nm. (d) HR-TEM image of 1 : 10 CdS/C core−shell composites with a carbon layer thickness of ~7 nm.

showing many carbon dots along with the carbon films formed by the pyrolysis of ascorbic acid.

As shown in Fig. 2a, Raman spectra of pure carbon materials with the excitation wavelength at 530 nm can be well fit with Gaussian functions, showing two characteristic bands at ~1413 cm^{-1} and ~1583 cm^{-1}, which are assigned to the D-band and G-band, respectively.[41,42] The G-band reveals the presence of graphite carbon, whereas the D-band is attributed to disorders or defects in the graphite structure,[43] indicating that the obtained pure carbon materials are graphitized to some extent.

Fig. 2b shows the UV-vis absorption spectrum of pure carbon in solution. The peak at ~285 nm can be assigned to the typical absorption of the π–π* transition of the conjugated C=C in nanocarbon materials,[44] which further indicates the formation of graphitized carbon. Generally, the carbon dots exhibit strong size and excitation wavelength dependent photoluminescence (PL) behaviors.[45] In Fig. 2c, the pure carbon materials contain-ing carbon dots indeed exhibit obvious dependence of PL on the excitation wavelength. The peak position of PL emission varies from 430 nm to 525 nm with the excitation wavelength shorter than 450 nm. According to Sun *et al.*, carbon dots can exhibit up-converted PL (UCPL).[46] In Fig. 2d, PL spectra of carbon materials with excitation at a longer wavelength (600–800 nm) also seem to show up-converted emission located from ~330 nm to ~460 nm in our experiment. These results all manifest the successful preparation of graphited carbon materials from the hydrothermal pyrolysis of ascorbic acid.

The comparison of Raman spectra between pristine CdS nanospheres and CdS/C composites is shown in Fig. 3. Pristine CdS exhibits the first-order longitudinal optical phonon (LO) at ~285 cm^{-1} and the second-order LO phonon peak at ~600 cm^{-1}.[33,47] However, when CdS was coated with a carbon layer, Raman spectra started to change, showing a broad spectral feature at ~1000 cm^{-1} instead of the characteristic peaks of carbon materials. This broad feature may be attributed to the synergistic interaction between CdS and the carbon layer, *e.g.* fluorescence of carbon materials. No characteristic carbon peaks at ~1413 cm^{-1} and ~1583 cm^{-1} can be observed due to the small amount of carbon layer.

The crystal structures of pristine CdS and CdS/C composites are determined using X-ray diffraction (XRD), as shown in Fig. 4a. All the diffraction peaks confirm the existence of a typical hexagonal phase of a wurtzite CdS structure (JCPDS card no. 75-1545).[12,48] No additional characteristic peaks from the carbon layer can be observed although there is an obvious carbon layer on the surface of CdS, which can be attributed to the amorphous nature of the carbon layer or the ultrathin layer of carbon and possible overlap between the peak expected at ~26° for carbon materials and the peak at ~25° of the (100) planes of CdS. The undifferentiated XRD patterns reveal that the formation of the carbon-coated CdS composites has a negligible effect on the crystal phase of CdS.

To further investigate the presence of the carbon layer in the CdS/C composites and the interaction between the carbon layer and the CdS nanosphere, Fourier transform infrared (FT-IR) spectroscopy and X-ray photoelectron spectroscopy (XPS) of pure carbon materials and CdS/C composites were carried out.

1080 | *J. Mater. Chem. A*, 2016, 4, 1078–1086

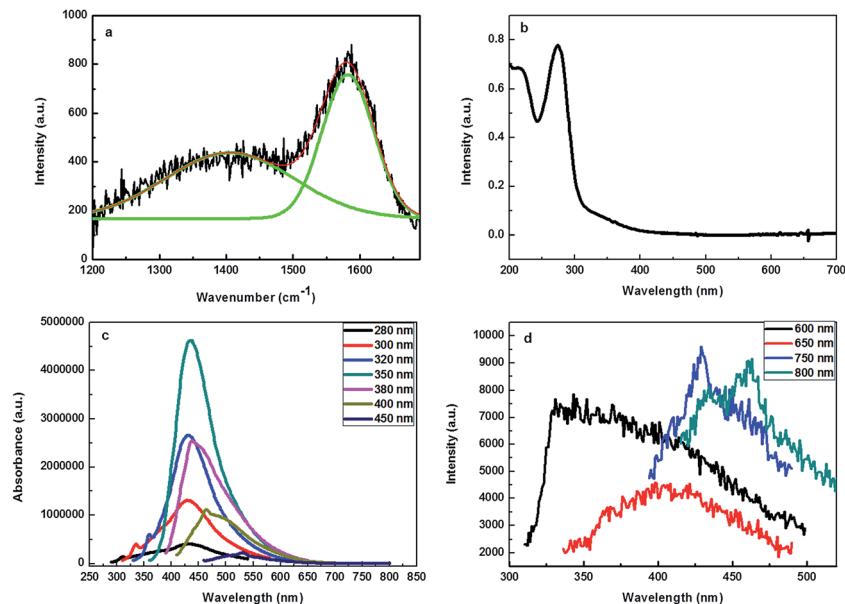This journal is © The Royal Society of Chemistry 2016

Fig. 2 (a) Raman spectra and (b) UV-vis absorption spectra of pure nanocarbon materials; (c) and (d) PL spectra of pure carbon materials in solution upon excitation at different wavelengths.
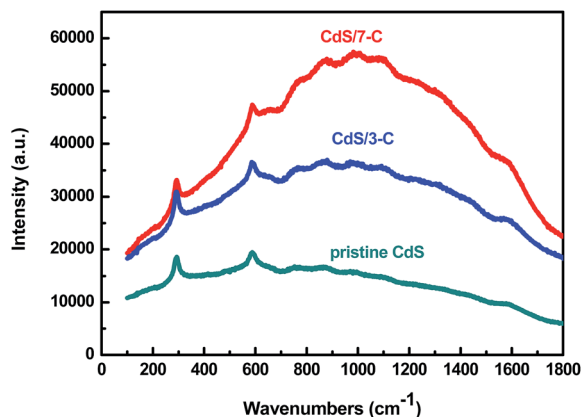

Fig. 3 Raman spectra of pristine CdS and CdS/C composites.

For pure carbon, as shown in Fig. 4b, the peak at $\sim$3368 cm^{-1} is assigned to the stretching vibration of the –OH group.[49] The peaks at $\sim$2943 cm^{-1} and $\sim$1702 cm^{-1} are ascribed to the stretch vibrations of –C–H and C=O bonds, respectively. Interestingly, the absorption peak at $\sim$1623 cm^{-1} due to C=O in carbon-coated CdS composites shows an obvious blue shift compared to that of pure carbon, possibly suggesting that partial ester groups [C(=O)O] have transformed into new Cd–COO groups in the carbon-coated CdS composites.[43] Absorption peaks at $\sim$2853 cm^{-1} and $\sim$2924 cm^{-1} corroborate the symmetric and asymmetric stretching vibrations of C–H bonds, respectively, which indicate the formation of the carbon layer on the CdS surface.[50]

Fig. 4c and d display the comparison of high-resolution C 1s XPS spectra for pure carbon materials and CdS/7-C composites, respectively. The C 1s spectrum of pure carbon can be deconvolved into three peaks located at $\sim$284.5 eV, $\sim$286.6 eV and $\sim$287.7 eV, which are assigned to C–C, C–O, and C=O, respectively.[51,52] Meanwhile, the C=O signal at $\sim$287.7 eV in pure carbon seems to shift to $\sim$288.4 eV in carbon-coated CdS composites (Fig. 4d and Table S1†), indicating the formation of new Cd–COO groups, which is consistent with the FT-IR results.

Comparison of the UV-vis spectra in Fig. 5a shows that the CdS/C composites exhibit enhanced absorption throughout the measured spectral range. All the samples show strong absorption in the visible light range, however, carbon-coated CdS composites show stronger absorption than that of pristine CdS nanoparticles at a wavelength longer than 510 nm, which indicates that the carbon layer may play important roles in utilizing sunlight. There is no characteristic peak at $\sim$285 nm from carbon materials, likely due to the small amount of carbon. The corresponding PL emission spectra are shown in Fig. 5b. For pristine CdS nanospheres, an emission peak at $\sim$523 nm is attributed to a bandgap transition in CdS. The carbon-coated CdS nanostructures show a similar PL spectrum but with a much weaker intensity compared with that of pristine CdS. The quenched PL in the composite is taken as an indication of photoinduced charge transfer from CdS to carbon.[53,54] The strong quenching suggests strong electronic interaction or coupling between CdS and the carbon layer.

In order to gain further insight into the charge transfer dynamics of CdS/C composites, ultrafast TA spectroscopy was utilized to investigate the charge carrier dynamics and their dependence on the carbon layer. In order to avoid non-linear dynamic processes and find the linear regime, pump power dependence of the dynamics in both CdS and CdS/C composites was carried out for three different pump powers of 1800 nJ per pulse, 780 nJ per pulse, and 90 nJ per pulse. The early time dynamics are found to be power dependent, indicating non-
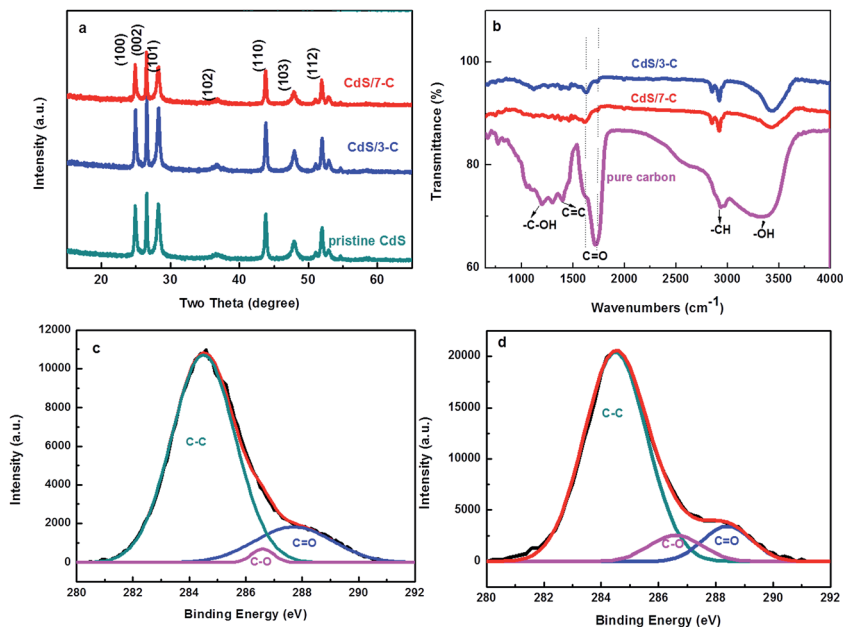
Fig. 4 (a) XRD patterns of pristine CdS and CdS/C composites; (b) FT-IR transmittance spectra of pure carbon materials and CdS/C composites; X-ray photoelectron spectroscopy (XPS) of (c) pure carbon materials and (d) CdS/7-C composites.
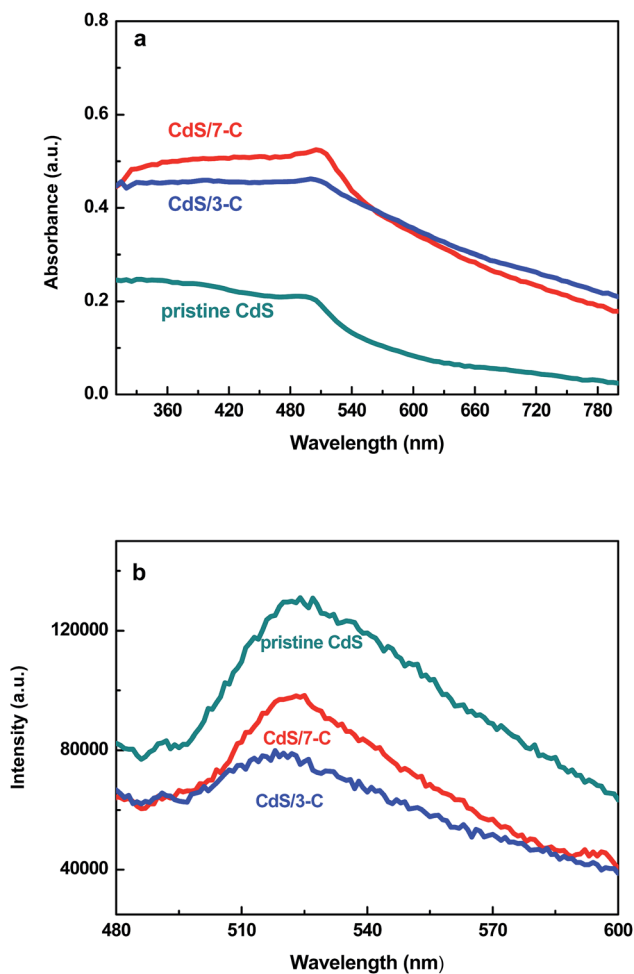

Fig. 5 (a) The UV-vis absorption spectra and (b) PL spectra of the pristine CdS and CdS/C composites.

linear dynamic processes at high power, *e.g.* exciton–exciton annihilation or Auger recombination often take place in quantum dots under high excitation intensity.[55] To remove or minimize the high-order, nonlinear processes, the lowest pump power at 90 nJ per pulse was chosen to compare the decay dynamics of CdS and CdS/C composites since the non-linear effect was minimal at this power.

Fig. 6 shows the contour plots of the TA data as a function of the probe wavelength and delay time between the pump and probe pulses with 400 nm excitation. The carbon materials do not have a detectable signature in the TA spectrum at this excitation wavelength because the excitation wavelength of 400 nm can only excite CdS. The intensity of differential absorption (dA) with and without the pump decreases with time delay between the pump and the probe over the probe wavelength range. For pristine CdS, the most obvious features are a broad transient absorption (TA) band from 450 nm–470 nm, which can be attributed to the absorption of photoexcited electrons in the CB (conduction band), and a symmetric transient bleach (TB) band with $\lambda_{max} = 504$ nm, which can be attributed to the hole absorption on the VB (valence band) of CdS. Carbon-coated CdS composites show similar profiles, however, the maxima of the bleach features of CdS/3-C and CdS/7-C are located at ~513 nm and ~495 nm, respectively. The red shift of TB profiles in carbon-coated CdS composites illustrates that the energy band structure of CdS could be varied after the coating of the carbon layer. In addition, for pristine CdS, the TB signal shows a symmetric peak from 500 nm to 550 nm, while CdS/C composites represent the broad TB feature and the tail to the longer wavelength (800 nm). This indicates that the carbon layer affects the excited state and/or ground state absorption. The UV-vis spectra in Fig. 5 show that the presence of carbon increases the extinction in the entire spectral range due to
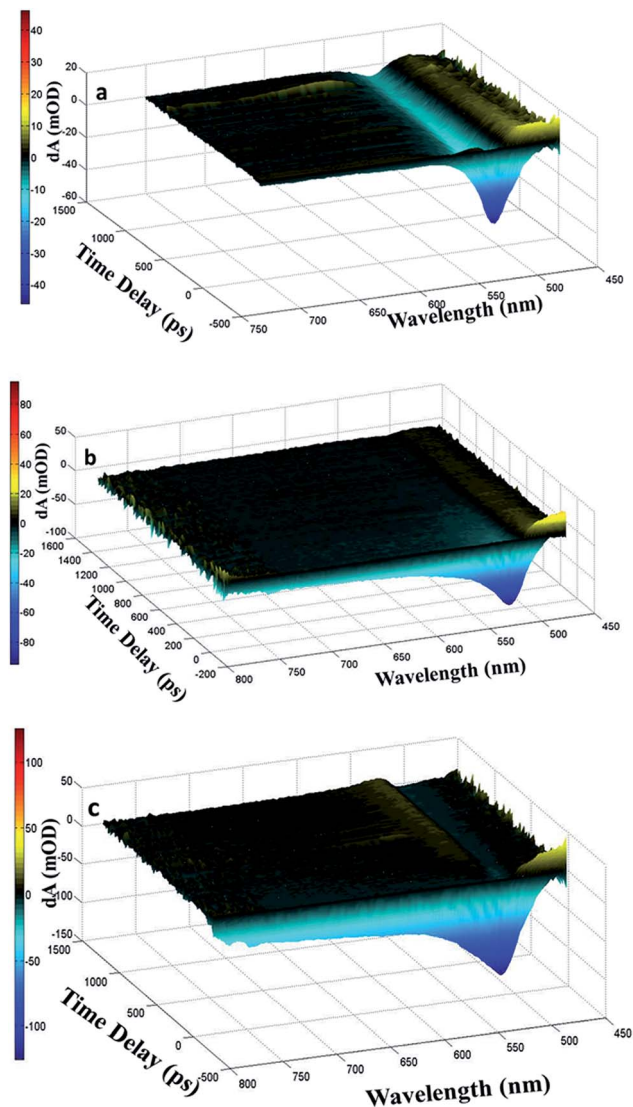
1082 | *J. Mater. Chem. A*, 2016, **4**, 1078–1086

This journal is © The Royal Society of Chemistry 2016

Fig. 6 Contour plots of the TA data for (a) pristine CdS; (b) CdS/3-C and (c) CdS/7-C excited with 400 nm light.
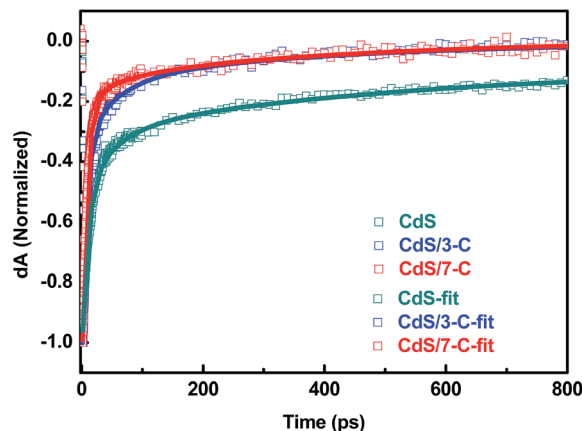

Fig. 7 The bleach decays and fitting results for the pristine CdS and CdS/C composites.

Table 1 Fitting results of the transient recovery dynamic profiles for pristine CdS and CdS/C composites at low (90 nJ per pulse) pump power

Samples	$A1$	τ_1 (ps)	$A2$	τ_2 (ps)	$A3$	τ_3 (ps)	$\bar{\tau}$ (ps)	k_{ET} (10^9 s^{-1})
CdS	0.56	10 ± 1	0.21	50 ± 9	0.22	528 ± 64	466	
CdS/3-C	0.97	8 ± 1	0.08	60 ± 9	0.13	434 ± 25	360	0.70
CdS/7-C	0.84	8 ± 1	0.20	58 ± 9	0.13	400 ± 16	303	1.20

increased absorption and/or scattering, which will increase the bleach signal and could result in the observed negative dA feature at a longer wavelength.

In order to better understand the charge carrier dynamics of CdS and CdS/C composites, the recoveries of normalized, single wavelength transient bleach dynamics for the three samples were analyzed in more detail, as shown in Fig. 7 (490 nm, 513 nm, and 495 nm for pristine CdS, CdS/3-C composites, and CdS/7-C composites, respectively). The TB recovery profiles can be fit with a triple-exponential function, and the fitting parameters are summarized in Table 1. The recovery lifetimes from the fitting results are 10 ± 1 ps, 50 ± 9 ps and 528 ± 64 ps for pristine CdS. According to previous studies of the exciton dynamics of the semiconductor nanocrystals or quantum dots (QDs), the fast and medium components can be usually attributed to exciton relaxation mediated by shallow and deep trap states, respectively, while the slow component is suggested

to the electron–hole recombination through the deep traps.[56] Meanwhile, the TB recovery profile of the CdS/3-C composite can be fit with 8 ± 1 ps, 60 ± 9 ps, and 434 ± 25 ps, while the TB profile of the CdS/7-C composite can be fit with 8 ± 1 ps, 58 ± 9 ps and 400 ± 16 ps. The overall recovery dynamics of the exciton or charge carriers appear faster for the CdS/C composites than that of pristine CdS, which can be attributed to the electron transfer from CdS to the carbon layer. This result is consistent with the quenched PL of CdS after the coating of the carbon layer (Fig. 5b).

To better understand the exciton dynamics of the CdS and CdS/C composites, an average lifetime is defined by the equation: $\bar{\tau} = \dfrac{A_1 \tau_1^2 + A_2 \tau_2^2}{A_1 \tau_1 + A_2 \tau_2}$, and calculated, which turned out to be 466 ps, 360 ps, and 303 ps for the pristine CdS, CdS/3-C composite, and CdS/7-C composite, respectively (i.e., CdS/7-C < CdS/3-C < pristine CdS). It is clear that the average lifetime is shorter for the CdS/C composites than that of pristine CdS. As summarized in Table 1, the amplitude of the fast recovery components ($A1\%$) increases and that of the slow component $A3\%$ decreases when the carbon layer is coated on the surface of CdS, which can be attributed to (1) the electron transfer from CdS to the carbon layer or (2) the increasing of the shallow states after the carbon layer coating. In order to further study the role of the carbon layer, the electron transfer rate constant is calculated using the equation: $k_{ET} = \dfrac{1}{\bar{\tau}_{C/CdS}} - \dfrac{1}{\bar{\tau}_{CdS}}$,[57] where $\bar{\tau}_{CdS}$ and $\bar{\tau}_{C/CdS}$ are

the average lifetimes of CdS and CdS/C electrodes, respectively. The electron transfer rates for CdS/3-C and CdS/7-C are determined to be 0.7×10^9 s^{-1} and 1.2×10^9 s^{-1}, respectively. These results suggest that the electron transfer from CdS to the carbon layer occurs on an ultrafast time scale, which suggests strong interaction between the carbon layer and CdS.

In general, the solar-to-hydrogen conversion efficiency is mainly determined by efficient light absorption and charge transport as for the application in photoelectrochemical (PEC) water splitting.[58] Hence, the PEC performance of pristine CdS and CdS/C composites as the photoanodes was investigated, as shown in Fig. 8. The photocurrent density–applied voltage (J–V) characteristics were measured under Xe lamp illumination. Fig. 8a shows that all of the electrodes display the negligible background current in the dark, indicating that no electrocatalytic oxygen evolution occurs. Among the three samples, CdS/7-C composites represent the highest PEC performance, and the photocurrent density can achieve a high value of ~0.47 mA cm^{-2} at -1.0 V vs. Ag/AgCl, which is almost 20 times higher than that of pristine CdS (0.025 mA cm^{-2}). In addition, the photocurrent density of CdS/3-C composites (0.30 mA cm^{-2}) exceeds that of pristine CdS by ~12 times. These results indicate that the CdS/C composites demonstrate a significant increase in the photoactivity compared with pristine CdS upon light illumination, which reveals the efficient charge separation in CdS/C composites. The onset potential of pristine CdS is ~-1.2 V (vs. Ag/AgCl), while it shifts to ~-1.4 V (vs. Ag/AgCl) for CdS/C composites. The decreased overpotential for CdS/C composites indicates effective interaction between CdS and the carbon layer.
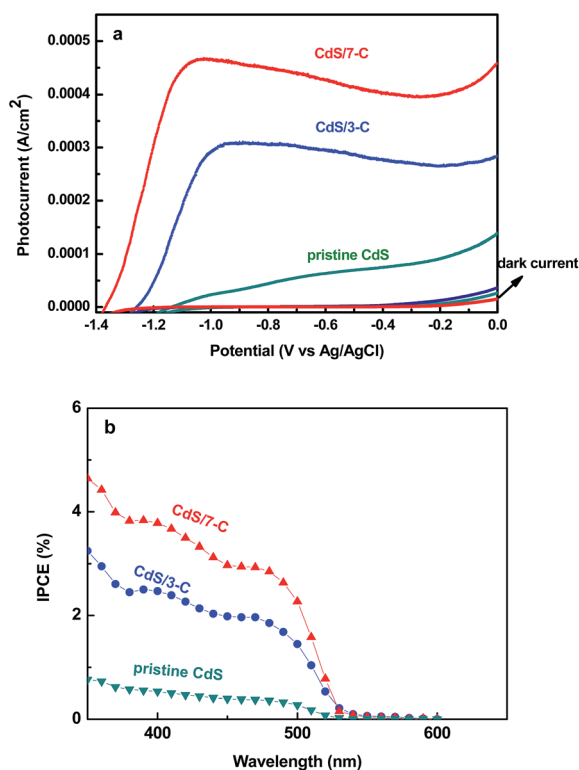
To further elucidate the role of the carbon layer in improved PEC performance, the incident photon-to-current efficiency (IPCE) spectra for pristine CdS and CdS/C composite electrodes are displayed at -0.5 V vs. Ag/AgCl as a function of the incident light wavelength in Fig. 8b. IPCE provides a reliable method to characterize the wavelength dependent photoresponse, and can be calculated by the equation: IPCE = $(1240I)/(\lambda J_{light})$, where I is the measured photocurrent density at a specific wavelength, λ is the wavelength of the incident light, and J_{light} is the measured irradiance at a specific wavelength.[58] The IPCE characteristics closely match the absorption spectrum of the individual electrodes. Both CdS/C composites show significantly improved photoactivity in the whole detected wavelength range in agreement with the results of PEC measurements, indicating that the carbon layer on the CdS can remarkably improve the PEC performance by efficient charge collection. These results show that a thin and uniform carbon layer on the surface of CdS nanospheres is indeed beneficial to enhance the PEC performance.

As discussed above, the enhanced PEC performance can be ascribed to the favorable morphology and excellent electronic conductivity of the carbon layer. In order to explain the role of the carbon layer in charge carrier dynamics, the model of CdS/7-C composites is illustrated in Fig. 9. The electrons in the valence band (VB) of CdS are excited to the conduction band by light with the energy higher than that of the bandgap, then the electrons can be trapped into shallow trap (ST) and deep trap (DT) states with a ~6 ps lifetime and a ~50 ps lifetime, respectively. And electrons in the CB and holes in VB states can undergo non-radiative recombination on the ~400 ps time scale by a non-radiative process. Some electrons can then be

Fig. 8 (a) Variation of J–V curves in the dark and under light illumination; IPCE spectra with wavelengths ranging from (b) 350 to 600 nm.
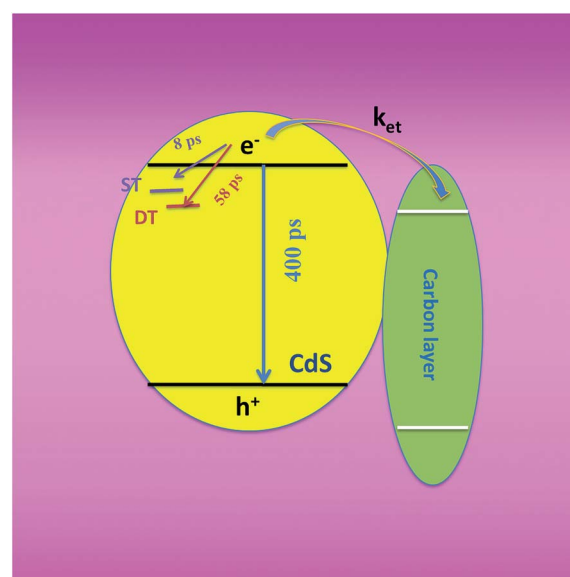

Fig. 9 Schematic illustration of charge carrier dynamics in CdS/7-C composites. The electrons can be trapped into shallow trap (ST) and deep trap (DT) states with a 6 ps lifetime and a 50 ps lifetime, respectively. And electrons in the CB and holes in VB states can undergo non-radiative recombination on the 400 ps time scale by a non-radiative process.

transferred to the surface of the carbon layer under the interface to achieve charge separation with $\bar{k}_{ET}$ of $1.2 \times 10^9 \, s^{-1}$. There are two main possibilities to explain the effective electron transfer. First, the carbon layer provides a homogeneous nanocoating on CdS, which can guarantee intimate and large contact interfaces between the CdS and the carbon layer, resulting in effective photogenerated electron transfer. Secondly, good electrical conductivity of the carbon layer ensures electron transfer between CdS and the carbon layer from all different directions. In particular, it highlights the importance of the carbon layer in effective electron collection in PEC performance.

4. Conclusions

In summary, uniform, complete and ultrathin carbon-coated CdS composites using ascorbic acid as the carbon source were fabricated by a facile hydrothermal method. The thickness of the carbon layer can be well adjusted by the amount of ascorbic acid during the reaction. The exciton and charge carrier dynamics of CdS and CdS/C composites were studied using transient absorption/bleach spectroscopy. The bleach decay profiles of pristine CdS, CdS/3-C composites and CdS/7-C composites were fit with a tri-exponential function, which produced an average lifetime of ~303 ps, ~360 ps, and ~466 ps, respectively. The overall faster decay of the CdS/C composites is attributed to the effective electron transfer from CdS to the carbon shell layer, which is uniform and forms a good interface with CdS. Meanwhile, the obtained CdS/C composites show strong PEC performance compared with pristine CdS. The enhanced photoactivity can be attributed to improved light absorption and efficient electron transfer. This novel and facile synthetic method of carbon-coated CdS nanostructures can be extended to fabricate other carbon-coated semiconductors at low temperature. Such nanocomposite structures are promising for photocatalytic and PEC applications.

Acknowledgements

References

1   A. Fernando, S. Parajuli and M. A. Alpuche-Aviles, *J. Am. Chem. Soc.*, 2013, **135**, 10894.

2   Y. Ling, G. Wang, D. A. Wheeler, J. Z. Zhang and Y. Li, *Nano Lett.*, 2011, **11**, 2119.

3   G. Hodes, D. Cahen and J. Manassen, *Nature*, 1976, **260**, 312.

4   L. Wang, C. Y. Lee and P. Schmuki, *J. Mater. Chem. A*, 2013, **1**, 212.

5   C. Zhen, L. Wang, G. Liu, G. Q. M. Lu and H. M. Cheng, *Chem. Commun.*, 2013, **49**, 3019.

6   A. Dabirian and R. van de Krol, *Chem. Mater.*, 2015, **27**, 708.

7   X. K. Zhao, L. McCormick and J. H. Fendler, *Chem. Mater.*, 1991, **3**, 922.

8   T. Y. Zhai, X. S. Fang, M. Y. Liao, X. J. Xu, H. B. Zeng, Y. Bando and D. Golberg, *Nanoscale*, 2009, **9**, 6504.

9   Y. F. Lin, J. Song, Y. Ding, S. Y. Lu and Z. L. Wang, *Adv. Mater.*, 2008, **20**, 3127.

10 Y. F. Lin, J. Song, Y. Ding, S. Y. Lu and Z. L. Wang, *Appl. Phys. Lett.*, 2008, **92**, 022105.

11 Y. Du, B. Chen, Z. Yin, Z. Liu and H. Zhang, *Small*, 2014, **10**, 4727.

12 S. C. Han, L. F. Hu, N. Gao, A. A. Al-Ghamdi and X. S. Fang, *Adv. Funct. Mater.*, 2014, **24**, 3725.

13 J. Yu, J. Jin, B. Cheng and M. Jaroniec, *J. Mater. Chem. A*, 2014, **2**, 3407.

14 Z. Wang, J. Hou, C. Yang, S. Jiao and H. Zhu, *Chem. Commun.*, 2014, **50**, 1731.

15 R. Lin, L. Shen, Z. Ren, W. Wu, Y. Tan, H. Fu, J. Zhang and L. Wu, *Chem. Commun.*, 2014, **50**, 8533.

16 X. J. Xu, L. F. Hu, N. Gao, S. X. Liu, S. Wageh, A. A. Al-Ghamdi, A. Alshahrie and X. S. Fang, *Adv. Funct. Mater.*, 2015, **25**, 445.

17 K. Wu, Z. Chen, H. Lv, H. Zhu, C. L. Hill and T. Lian, *J. Am. Chem. Soc.*, 2014, **136**, 7708.

18 J. Li, S. K. Cushing, P. Zheng, T. Senty, F. Meng, A. D. Bristow, A. Manivannan and N. Wu, *J. Am. Chem. Soc.*, 2014, **136**, 8438.

19 Y. Wang, H. Li, P. He, E. Hosono and H. Zhou, *Nanoscale*, 2010, **2**, 1294.

20 D. Bresser, E. Paillard, R. Kloepsch, S. Krueger, M. Fiedler, R. Schmitz, D. Baither, M. Winter and S. Passerini, *Adv. Energy Mater.*, 2013, **3**, 513.

21 W. M. Zhang, J. S. Hu, Y. G. Guo, S. F. Zheng, L. S. Zhong, W. G. Song and L. J. Wan, *Adv. Mater.*, 2008, **20**, 1160.

22 X. Tong, P. Yang, Y. Wang, Y. Qin and X. Guo, *Nanoscale*, 2014, **6**, 6692.

23 H. Zhang, X. Lv, Y. Li, Y. Wang and J. Li, *ACS Nano*, 2009, **4**, 380.

24 Q. Xiang, J. Yu and M. Jaroniec, *Chem. Soc. Rev.*, 2012, **41**, 782.

25 Y. Zhang, N. Zhang, Z. R. Tang and Y. J. Xu, *ACS Nano*, 2012, **6**, 9777.

26 N. Li, G. Liu, C. Zhen, F. Li, L. Zhang and H. M. Cheng, *Adv. Funct. Mater.*, 2011, **21**, 1717.

27 F. X. Xiao, J. Miao and B. Liu, *J. Am. Chem. Soc.*, 2014, **136**, 1559.

28 K. Chang, Z. Mei, T. Wang, Q. Kang, S. Ouyang and J. Ye, *ACS Nano*, 2014, **8**, 7078.

29 X. Wang, X. Cao, L. Bourgeois, H. Guan, S. Chen, Y. Zhong, D. M. Tang, H. Li, T. Zhai and L. Li, *Adv. Funct. Mater.*, 2012, **22**, 2682.

30 S. Sim, P. Oh, S. Park and J. Cho, *Adv. Mater.*, 2013, **25**, 4498.

31 N. Li, G. Zhou, F. Li, L. Wen and H. M. Cheng, *Adv. Funct. Mater.*, 2013, **23**, 5429.

32 G. Gao, H. B. Wu, S. Ding and X. W. Lou, *Small*, 2014, **11**, 432.

33 Y. Hu, X. Gao, L. Yu, Y. Wang, J. Ning, S. Xu and X. W. Lou, *Angew. Chem.*, 2013, **125**, 5746.

34 J. Wang and X. Sun, *Energy Environ. Sci.*, 2012, **5**, 5163.

35 H. Li and H. Zhou, *Chem. Commun.*, 2012, **48**, 1201.

36 F. Wu, J. H. Yu, J. Joo, T. Hyeon and J. Z. Zhang, *Opt. Mater.*, 2007, **29**, 858.

37 T. Jia, A. Kolpin, C. Ma, R. C. T. Chan, W. M. Kwok and S. E. Tsang, *Chem. Commun.*, 2014, **50**, 1185.

38 J. Zhang, L. Qi, J. Ran, J. Yu and S. Z. Qiao, *Adv. Energy Mater.*, 2014, **4**, 1301925.

39 C. Han, Z. Chen, N. Zhang, J. C. Colmenares and Y. J. Xu, *Adv. Funct. Mater.*, 2015, **25**, 170.

40 S. Dutta, R. Sahoo, C. Ray, S. Sarkar, J. Jana, Y. Negishi and T. Pal, *Dalton Trans.*, 2015, **44**, 193.

41 L. V. Frolova, I. V. Magedov, A. Harper, S. K. Jha, M. Ovezmyradov, G. Chandler, J. Garcia, D. Bethke, E. A. Shaner and I. Vasiliev, *Carbon*, 2015, **81**, 216.

42 R. Beams, L. G. Cançado and L. Novotny, *J. Phys.: Condens. Matter*, 2015, **27**, 083002.

43 J. Yang, J. Wang, Y. Tang, D. Wang, X. Li, Y. Hu, R. Li, G. Liang, T. K. Sham and X. Sun, *Energy Environ. Sci.*, 2013, **6**, 1521.

44 X. Chen, W. Zhang, Q. Wang and J. Fan, *Carbon*, 2014, **79**, 165.

45 J. Bian, C. Huang, L. Wang, T. Hung, W. A. Daoud and R. Zhang, *ACS Appl. Mater. Interfaces*, 2014, **6**, 4883.

46 L. Cao, X. Wang, M. J. Meziani, F. Lu, H. Wang, P. G. Luo, Y. Lin, B. A. Harruff, L. M. Veca and D. Murray, *J. Am. Chem. Soc.*, 2007, **129**, 11318.

47 R. Kostić and N. Romčević, *Phys. Status Solidi C*, 2004, **1**, 2646.

48 G. Bertoni, V. Grillo, R. Brescia, X. Ke, S. Bals, A. Catellani, H. Li and L. Manna, *ACS Nano*, 2012, **6**, 6453.

49 Z. X. Chi, W. Zhang, X. S. Wang, F. Q. Cheng, J. T. Chen, A. M. Cao and L. J. Wan, *J. Mater. Chem. A*, 2014, **2**, 17359.

50 S. Yuvaraj, S. Amaresh, Y. Lee and R. K. Selvan, *RSC Adv.*, 2014, **4**, 6407.

51 Y. Zhang, Z. R. Tang, X. Fu and Y. J. Xu, *ACS Nano*, 2011, **5**, 7426.

52 S. Prezioso, F. Perrozzi, L. Giancaterini, C. Cantalini, E. Treossi, V. Palermo, M. Nardone, S. Santucci and L. Ottaviano, *J. Phys. Chem. C*, 2013, **117**, 10683.

53 Z. B. Yu, Y. P. Xie, G. Liu, G. Q. M. Lu, X. L. Ma and H. M. Cheng, *J. Mater. Chem. A*, 2013, **1**, 2773.

54 Y. Hu, H. Qian, Y. Liu, G. Du, F. Zhang, L. Wang and X. Hu, *CrystEngComm*, 2011, **13**, 3438.

55 D. A. Wheeler and J. Z. Zhang, *Adv. Mater.*, 2013, **25**, 2878.

56 J. K. Cooper, Y. Ling, C. Longo, Y. Li and J. Z. Zhang, *J. Phys. Chem. C*, 2012, **116**, 17360.

57 Y. C. Pu, W. H. Lin and Y. J. Hsu, *Appl. Catal., B*, 2015, **163**, 343.

58 Q. Gui, Z. Xu, H. Zhang, C. Cheng, X. Zhu, M. Yin, Y. Song, L. Lu, X. Chen and D. Li, *ACS Appl. Mater. Interfaces*, 2014, **6**, 17053.